Microstructural change of nano-SnO_2 grain assemblages with the annealing temperature

K. N. Yu
Department of Physics and Materials Science, City University of Hong Kong, Kowloon, Hong Kong

Yonghong Xiong
Department of Physics and Materials Science, City University of Hong Kong, Kowloon, Hong Kong and Foundational Physics Center, University of Science and Technology of China, Chinese Academy of Science, Hefei, Anhui, 230026, People's Republic of China

Yulong Liu
Institute of Physics, Chinese Academy of Science, Beijing, 100080, People's Republic of China

Caoshui Xiong
Structure Research Laboratory, University of Science and Technology of China, Chinese Academy of Science, Hefei, Anhui, 230026, People's Republic of China

(Received 1 April 1996; revised manuscript received 11 June 1996)

The microstructural changes of nano-SnO_2 have been systematically studied using x-ray diffraction and Raman spectroscopy. The nano-SnO_2 grain assemblage possesses some features of the rutile structure, but has a large amount of defects: vacancies of oxygen, vacancy clusters, and local lattice disorder at the interface and interior surface, which lead to a significant lattice distortion and an evident space-symmetry reduction of D_{4h}^{14} and the appearance of a group of new Raman peaks. Two major Raman peaks N_1 and N_2 in accordance with Matossi's force constant model have been found. When the annealing temperature is close to 673 K, the density of vacant lattice sites and local lattice disorders decreased rapidly in the grains, and the lattice distortion and Raman peaks N_1 and N_2 almost disappeared at the same time. It suggests that N_1 and N_2 are closely related to the microstructural change of the nanocluster grains, or in other words, N_1 and N_2 peaks mark an additional characteristic of space symmetry of the grain assemblage of nano-SnO_2. The Raman peak N_3 may be related to local SnO_2 clusters and vacancy clusters. [S0163-1829(97)09704-X]

I. INTRODUCTION

The peculiar structure and the unusual physical and chemical properties of nanomaterials have recently aroused a great deal of interest. Generally speaking, the nanostructural materials are made of two main components, i.e., a grain component including nanocrystallite, nanocluster assemblages, nanoamorphous grains, etc., and an interface component formed by large interfaces and surfaces, etc.

The interface and surface structure have been widely studied. Various types of interface-structure models have been proposed for nanostructural materials,[1–6] such as the gaslike model, order and extended order models, and ones with a distribution of structural features. It is common that the various peculiar properties of nanomaterials are explained in terms of the interface and surface structure, while the effects from the internal microstructure of the grains are neglected. In fact, for different preparation methods the microstructure of nanomaterials can be nanocrystallite, nanoamorphous grain, or nanocluster assemblages with some crystal feature. Since the grains are the basic components of nanomaterials, changes in their internal microstructure should inevitably change the physical and chemical properties. Therefore, the study of the internal microstructure of the grains can help us reveal the general structure of nanomaterials and explain the corresponding experimental results.

X-ray diffraction (XRD) is a powerful tool commonly employed in the studies of the structure of materials. For nanomaterials, it is common to use XRD to determine the crystal structure and to roughly estimate the mean-grain size, including the variation of the grain size with annealing temperature. Only in the past few years have a few papers reported[7,8] the use of XRD for more detailed studies of the lattice distortion in nanomaterials and the change in the microstructure with annealing temperature. On the other hand, Raman spectroscopy is a powerful tool used to reveal the space symmetry of materials. The use of XRD and Raman spectroscopy together might enhance our understanding of the signals from the microstructural change and various defect states in nanomaterials.

SnO_2 is a stable large band-gap oxide semiconductor which has excellent photoelectronic properties and sensitivities of gases, etc.[9–13] In nano-SnO_2, the above properties have been extensively explored,[14–17] and nano-SnO_2 will find wide applications in microelectronics, photoelectronics, sensor and compound function ceramics. The attempt to improve its properties largely relies on the understanding of the microstructure of nano-SnO_2. In the present work, we have studied the relationships between the microstructural change of grains and the change of space symmetry with the annealing temperature of nano-SnO_2, and have discussed the reasons behind the lattice distortion.

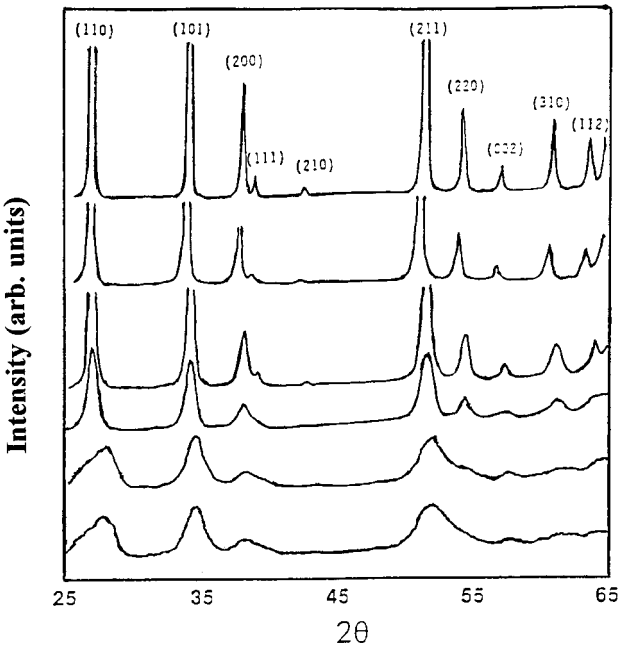

FIG. 1. XRD spectra of nano-SnO_2 with different annealing temperature T_a. From bottom to top: unannealed; $T_a = 473$, 673, 873, 1073, 1273 K.

II. EXPERIMENTAL RESULTS AND DISCUSSION

The nano-SnO_2 grains with an average grain diameter smaller than 4 nm have been prepared by the hydrothermal method.[18,19] Nitric acid is mixed with 0.25 mol/L solution of SnC_{14} in a suitable ratio, which is heated to 150 °C for 12 h in a sealed hyperbaric vessel cushioned with polytetrafluoroethylene and then cooled naturally to room temperature. The product is washed repeatedly with deionized water and absolute acetone alternatively and the white nano-SnO_2 powder is obtained. The powder is dried in a vacuum desiccator and then stored in a desiccator. Under a pressure of 200 MPa, the nano-SnO_2 powder is pressed to form circular discs with a diameter of about 10 mm and a thickness of about 1 mm. Samples of different grain size are made using different isothermal annealing at 473, 673, 873, 1073, and 1273 K for 6 h. X-ray diffraction patterns were obtained with a Japan Rigaku D/mex-ra rotating x-ray diffractometer using Cu $K\alpha$ radiation, with an operating voltage of 40 kV and a current of 100 mA. The feature micrographs were obtained using the H-900 transmission electron microscope. The average size of nano-SnO_2 grain was measured and determined by XRD and transmission electron microscopy (TEM) and Raman spectra were obtained at room temperature using the Raman spectrometry system consisting of the SPEX-1403 double monochromator with holographic gratings, a cooled Hamamatsu R928 photomultiplier with photon counting electronics, and a DMIA Processor-Controller for data acquisition, instrumental control, and data analysis. The excitation source was an argon-ion laser of 480 nm in the backscattering configuration and the resolution of the instrument was 2 cm^{-1}.

The XRD spectra and the spacing of indices in the direct lattice of nano-SnO_2 with different annealing temperatures have been shown in Fig. 1 and Table I. The average grain size is calculated using the TEM micrograph and the Scherrer formula, respectively. Both results show that the average grain size of the unannealed sample is about 4 nm. The grain size of samples with different annealing temperatures are 4, 8, 20, 40, and 80 nm.

From Fig. 1 and Table I, we see that for the unannealed sample, there are five rather broad diffraction peaks whose positions have shifted and whose relative intensities have changed when compared with the data in the literature.[20] With increasing annealing temperatures, the diffraction peaks are sharpened and enhanced, thereby indicating that the particles have grown and the crystal quality has been improved. For the tetragonal structure, the lattice parameter can be calculated by

TABLE I. The relation between $d^*_{(hkl)}$ and the annealing temperature of nano-SnO_2, where $d^*_{(hkl)}$ is the spacing of index (hkl) in the direct lattice. I/I_0 are the relative intensities of XRD peaks, T_a the annealing temperatures (K), and D the average grain size (nm).

Sample [a]	n-1	n-2	n-3	n-4	n-5	n-6	7#		
Ta (K)	unannealed	473	673	873	1073	1273			
D (nm)	4	4	8	20	40	80	μm		
$d^*_{(hkl)}$	d (Å)	d (Å)	d (Å)	d (Å)	d (Å)	d (Å)	d (Å)	I_1/I_0 (%)	I_7/I_0 (%)
110	3.300	3.300	3.351	3.350	3.370	3.351	3.351	100	100
101	2.652	2.650	2.648	2.644	2.659	2.637	2.644	90	81
200	2.394	2.390	2.374	2.368	2.380	2.366	2.369	25	24
111				2.298	2.300	2.304	2.309		5
210				2.129	2.118	2.117	2.120		2
211	1.759	1.760	1.761	1.763	1.768	1.762	1.765	100	63
220			1.678	1.675	1.681	1.672	1.675		63
002	1.612	1.610	1.610	1.610	1.610	1.590	1.593	10	8
310			1.499	1.498	1.501	1.497	1.498		13
112		1.430	1.431	1.439	1.443	1.439	1.439		17

[a]Nano-SnO_2 samples with serial numbers n-1 to n-6 with different annealing temperatures. 7# refers to the data in the literature (Ref. 20).

TABLE II. The relation between lattice parameters and the annealing temperature of nano-SnO_2. [a_{110} and a_{200} are calculated with XRD peaks (110) and (200), respectively; $c_{101\text{-}110}$ and $c_{101\text{-}200}$ are calculated with XRD peaks (101), (110), and (200), respectively; Δa and Δc are the difference of a_{110} and a_{200}, and $c_{101\text{-}200}$, respectively.]

Sample	n-1	n-2	n-3	n-4	n-5	n-6	7#
$\overline{D}$ (nm)	4	4	8	20	40	80	μm
T_a (K)	unannealed	473	673	873	1073	1273	
a_{110} (Å)	4.677	4.677	4.739	4.738	4.766	4.739	4.739
a_{200} (Å)	4.788	4.780	4.784	4.736	4.760	4.732	4.738
Δa (Å)	−0.121	−0.113	−0.009	0.002	0.006	0.007	0.001
$c_{101\text{-}110}$ (Å)	3.223	3.219	3.193	3.186	3.204	3.174	3.186
$c_{101\text{-}200}$ (Å)	3.185	3.187	3.190	3.187	3.206	3.176	3.186
Δc (Å)	0.038	0.033	0.003	−0.001	−0.002	−0.002	0.000

$$\frac{1}{d_{hkl}^2}=\frac{h^2+k^2}{a^2}+\frac{l^2}{c^2}, \tag{1}$$

where h, k, and l are all integers, (hkl) is the lattice plane index, and a and c are lattice constants. For a real crystal, the calculated values of a and c are the same based on different crystal planes. However, the presence of a large number of vacant lattice sites and local lattice disorders may lead to serious reduction in the intensity (or even the nearly disappearance) of the XRD peaks of the corresponding lattice plane [e.g., the lattice plane (220)]. In the standard spectrum database for SnO_2, that peak has a relatively intensity of 63%, and is one of the four strongest characteristic peaks (see Table I). On the other hand, the weak peaks (200) and (002), with relative intensities 24% and 8% in the standard spectrum have essentially kept their relative intensities. Our results therefore suggest destroyed periodicities in some crystal planes and a significant distortion of the rutile lattice. We have calculated the lattice parameters with different annealing temperatures using Eq. (1). The results have been shown in Table II and Fig. 2.

From Fig. 2, we can easily notice the relationships of the annealing temperature with the changes of lattice parameters, and with the volume fractions of interfaces. The volume fractions of interfaces V_i can be calculated by[21] $V_i=3\Delta/D$, where Δ is the average thickness of the interface or surface and D is the average diameter of the nano-SnO_2 grains. There are a large number of vacancies of oxygen, vacancy clusters, and local lattice disorders, which lead to an increase in c and decreases in a and the volume of the unit cell. The low-temperature annealing can lead to a relaxation in the interface structure, but cannot dispel the local lattice disorders or change the internal structure of the nanograins, so there are no apparent changes in the positions and intensities of XRD peaks. When the annealing temperature T_a is close to 673 K, there is a rapid decrease in the density of vacant lattice sites, vacancy clusters, and local lattice disorders and a rapid resumption of lattice parameters and the volume of the unit cell towards normal values, and the grains begin to grow. From room temperature to 673 K, Δa increases while Δc decreases by almost an order of magnitude, and at the same time, the volume fraction of interfaces decreases from 52% to 26%. When T_a is higher than 873 K, the vacancies can assemble and form vacancy clusters in the interface, which leads to a local state of interface. The unit cell volume increases since the SnO_2 cluster and vacancy clusters get into the lattice when T_a increases and the grains grow ($\Delta v/v$ is about 1.7% for annealing at 1073 K for 6 h). When T_a is higher than 1273 K, the density of vacancy clusters decreases rapidly and the cell volume resumes its normal value.

It is well known that in a substable fluid phase, single atoms or molecules will turn into atoms or molecules of stable grain phase, which will decrease the Gibb's free en-

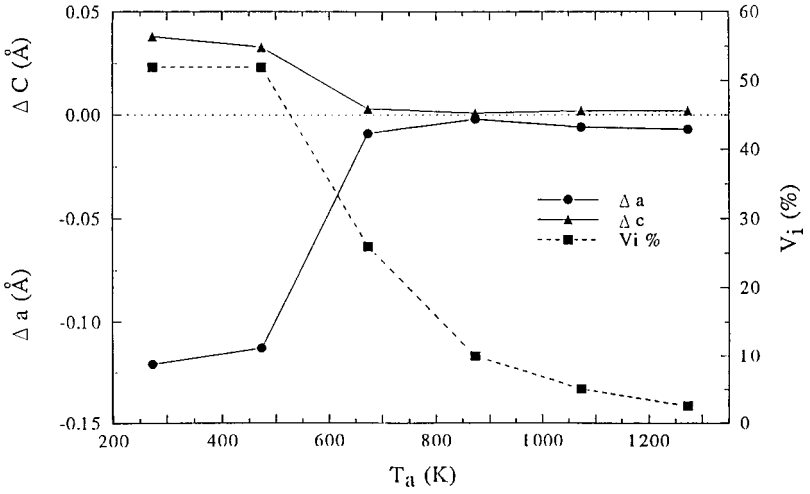

FIG. 2. The relationships of the annealing temperature with the changes in lattice parameters and the volume fractions of interface.

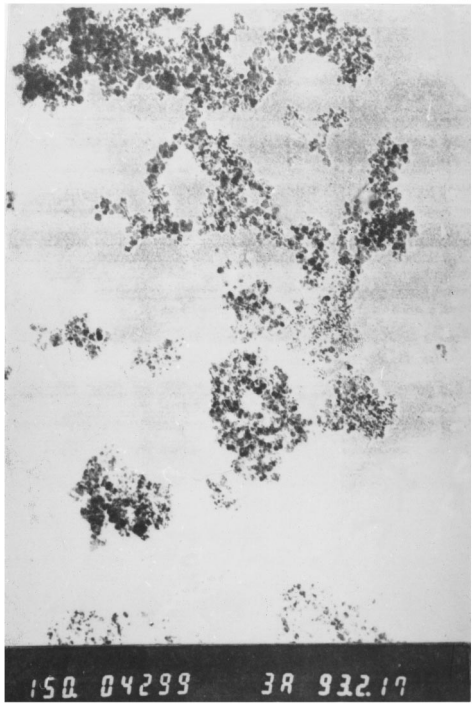

FIG. 3. TEM featured micrograph of nano-SnO_2 (sample No. n-1, $\times 150\,000$).

ergy ΔG. If the volume of an atom or molecule of grain is Ω_s, the interfacial energy between the crystal and the fluid is γ_{sf}, and the radius of a spherical assembled grain formed in the substable fluid is r, the resulted change of the Gibb's free energy is

$$\Delta G(r)=\frac{4\pi r^3}{3\Omega_s}\Delta g+4\pi r^2\gamma_{sf}. \tag{2}$$

If the spherical grain with the radius r is composed of i atoms or molecules, ΔG can be expressed as a function of i to give the general expression

$$\Delta G(i)=i\Delta g+A(i)\gamma_{sf}, \tag{3}$$

where $A(i)$ is the volume fraction of interfaces, namely, $A(i)=\eta I^{2/3}$, and η is the form factor which is given by $\eta=(36\pi)^{1/3}\Omega_s^{2/3}$ for a spherical grain and $\eta=6\Omega_s^{2/3}$ for a cubic one.

When the size of a grain is greater than the micrometer range, its shape will depend on the dynamics of the crystal growth process. When the size is several nm, the main factor deciding its shape may be the requirement of a minimum interfacial energy. For fluids, the energy for a spherical interface is minimum; for crystals, the external crystal face is the crystal face having the lowest interfacial energy. Therefore, during the formation of nano-SnO_2, in order to maintain the minimum energy of the system, spherical crystals need to be formed and the crystal face should be the one which possesses the lowest interfacial energy for the assembled grains. The feature micrograph of the 4-nm sample is shown in Fig. 3. For the convenience of calculation and description, we describe the crystals as nearly spherical. This

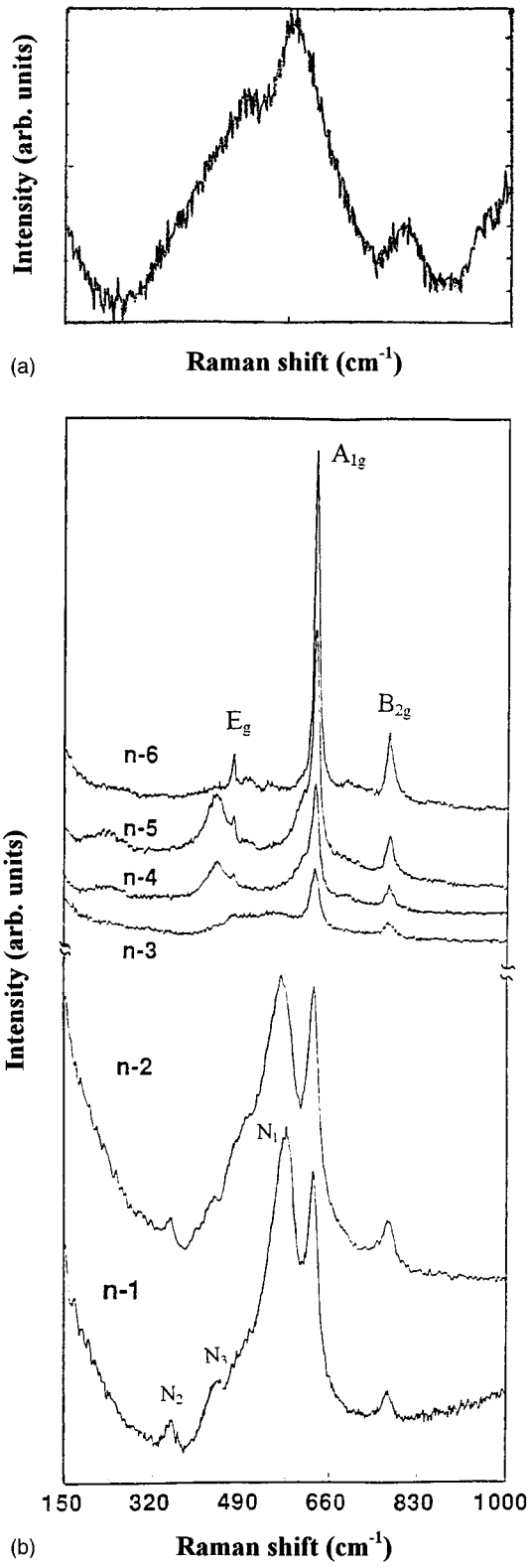

FIG. 4. Raman spectra at room temperature of (a) an amorphous film of SnO_2 (Sample No. a-0), and (b) nano-SnO_2 sample with different annealing temperatures (Sample Nos. n-1 to n-6).

is supported by the high-resolution electron microscope photograph of SnO_2 obtained in Ref. 6 which showed that the crystals are polygons, most of which tend to be spherical. In the grains, a defect (such as vacant lattice site, vacancy clus-

TABLE III. Raman spectra vibration modes of SnO_2. Data with (*) are data from Refs. 22–25, while those with (**) are calculated using Eq. (5). N_1 to N_3 represent new Raman peaks. VS: very strong vibration; *S*: strong; *M*: medium strong; *W*: weak.

Mode	Ref. 22 (cm^{-1})	Ref. 23 (cm^{-1})	Ref. 24 (cm^{-1})	Ref. 25 (cm^{-1})	Our data (cm^{-1})						
					a-0	n-1	n-2	n-3	n-4	n-5	n-6
A_{1g}	632	638	639.6*	634		630_S	630_S	630_S	630_{VS}	630_{VS}	630_{VS}
A_{2g}	455*	398*									
B_{1g}	87	100*	126.6*	184*							
B_{2g}	773	782	760.8*	777	788_W	774_M	774_M	774_M	774_M	774_M	774_M
E_g	472	476	451.4*	475				472_M	472_M	472_M	472_M
N_1						574**	569**				
					566_S	574_{VS}	568_{VS}				
N_2						358_M	350_M				
N_3						440_M	440_M		442_M	442_M	

ter, or local disorder) causes the lattice distortion and the lowering of lattice space symmetry.

A unit cell of the typical rutile structure of SnO_2 contains two tin ions and four oxygen ions and belongs to the space group $D_{4h}^{14}(P_{42/mnm})$. Scott,[22] Katiyar *et al.*,[23] Sato *et al.*,[24] and Gervais and Kress[25] have investigated the vibration spectrum of single-crystal SnO_2. According to the group theory, there are 15 lattice vibration modes:

$$G_{\text{rutil}}=A_{1g}+A_{2g}+A_{2u}+B_{1g}+B_{2g}+2B_u+E_g+3E_u, \tag{4}$$

where A_{1g}, B_{1g}, B_{2g}, and E_g are Raman active. A_{2u} and E_u possess TO and LO mode, where TO is transverse-optical vibration and LO is longitudinal-optical vibration.

Figure 4 and Table III show the Raman spectra vibration modes of a single crystal, an amorphous film having the sample serial number (a-0), and six nano-SnO_2 samples with different annealing temperatures having the serial numbers (n-1) to (n-6). Clearly, the peaks of nano-SnO_2 in the Raman spectra can be divided into two groups. One group resembles the vibration modes of microcrystal and single crystal SnO_2 (we refer to them as the *C* peaks). These Raman shifts are 630, 774, and 472 cm^{-1}, which are consistent with the A_{1g}, B_{2g}, and E_g vibration modes, respectively. A_{1g} (630 cm^{-1}) and B_{2g} (774 cm^{-1}) are related to the expansion and contraction vibration mode of Sn-O bonds, while E_g is related to the vibration of oxygen in the oxygen plan. These peaks show that the nano-SnO_2 possess the main characteristic of the tetragonal rutile structure. In the n-1 sample, besides the previous peaks, we have also found other group Raman shifts of 358, 574, and 440 cm^{-1} (we refer to them as the *N* peaks). The *N* peaks have not been observed in Raman spectra of single crystal or microcrystal SnO_2, but N_1 is close to the vibration mode (566 cm^{-1}) of an amorphous film of SnO_2. It is evident that the positions of the two new peaks shift towards lower frequencies and the relative intensities change for isothermal annealing at 473 K for 6 h. We study N_1 and N_2 according to the Matossi force constant model[20,26] using

$$\omega(N_1)=[\omega^2(N_2)+\omega^2(B_{2g})+\omega^2(A_{1g})]^{1/2} \tag{5}$$

and have found that the data from calculations agree very well with our Raman spectra (see Table III).

We attribute the above phenomena and results to the microstructure of components of nano-SnO_2. First, the *N* peaks are closely related to the microstructure of the nanocluster grains; they might constitute a new kind of vibration mode according to Matossi's force constant model, reflecting a new characteristic of space symmetry of the nano-SnO_2 grain assemblage which is closely related to vacant lattice sites and local lattice disorder, or they might be related to A_{2g} and B_{1g}. B_{1g} is of the greatest interest in the four Raman-active modes while A_{2g} is Raman inactive. Scott[22] determined B_{1g} to be 87 cm^{-1} and calculated A_{2g} to be 455 cm^{-1} using Eq. (5). A_{2g} and B_{1g} modes are related to the linear O-Sn-O base which turns around the vertical axis of Sn, and the B_{1g} mode is related to an incipient instability in the lattice.[22] For a nano-SnO_2 grain assemblage, a large number of vacant lattice positions and local lattice disorders can lead to a change in the bond length, a space symmetry reduction of D_{4h}^{14}, and a serious lattice distortion. In particular, the vacancy of oxygen and local disorder in the lattice plane (220) may shift the vibrational frequency of B_{1g} and transform A_{2g} into Raman active. If we assume the vibrational frequency of B_{1g} shifts to 358 and 350 cm^{-1}, the vibrational frequency of A_{2g} will be 574 and 569 cm^{-1} from Eq. (5) for samples $n-1$ and $n-2$, respectively.

Second, N_1 and N_2 may be related to the structure of the interface component.[27,28] The degree of order of interface atoms can affect the relative linewidth and positions of N_1 and N_2 peaks. The N_3 peak may be related to vacancy clusters and local SnO_2 clusters. When the samples are annealed isothermally at 673 K for 6 h, the new Raman peaks almost disappear and the intensity of the A_{1g} peak increases while the linewidth decreases due to the disappearance of the vacant lattice sites and local lattice disorders. At the same time, the lattice distortion almost disappears and all XRD peaks can be identified with Cohen's tetragonal rutile structure of SnO_2. As the isothermal annealing temperature increases, the grain size increases and all XRD peaks and *C* peaks of Raman spectra become more intense and sharp. Due to the assemblage of interface vacancies and the resulting rapid increase of vacancy clusters, and due to the emergence of a local SnO_2 cluster in the interface, the N_3 mode is once again excited. Its intensity increases and its linewidth broadens probably because the densities of vacancy clusters and

local SnO_2 clusters increase and some of them become incorporated into the lattice. When the annealing temperature is higher than 1273 K, part of the vacancy clusters integrate with local SnO_2 clusters. Together with the crystal growth and perfection, a portion of the vacancy clusters evolve into nanoholes, the local states rapidly decrease and the N_3 peaks disappear.

To sum up, we suggest that the main reasons behind the change of some diffraction peaks and the emergence of new Raman peaks are the microstructural change of the grain component and the lowering of the lattice space symmetry, in addition to the effects at the interface and surface. The N_1 and N_2 peaks agree fairly well with the Matossi force constant model. The lattice distortion almost disappears and the space symmetry reverts to D_{4h}^{14} when the samples are annealed isothermally at 673 K for 6 h. The study of the change of the internal microstructure of the grains is significant for the understanding of the whole structural feature of nanomaterials and for the preparation of new nanomaterials with peculiar properties.

[1] H. Gleiter *et al.*, Mater. Sci. Eng. **52**, 91 (1982); Phys. Rev. B **35**, 9085 (1987).
[2] H. E. Schaefer *et al.*, Phys. Rev. B **38**, 9545 (1988).
[3] H. Gleiter, Nanostruct. Mater. **1**, 1 (1992).
[4] G. Skandan *et al.*, Nanostruct. Mater. **1**, 313 (1992).
[5] W. Wunderlich *et al.*, Scr. Metall. Mater. **24**, 403 (1990).
[6] D. Z. Wang *et al.*, Phys. Rev. B **49**, 14 282 (1994).
[7] J. A. Eastman, J. Appl. Phys. **75**, 770 (1994).
[8] X. D. Liu *et al.*, Chin. Sci. Bull. **39**, 217 (1994).
[9] T. Miyasaka *et al.*, Nature **277**, 836 (1979).
[10] H. Ogawa *et al.*, J. Electrochem. Soc. **128**, 2020 (1981).
[11] A. Reis, Helv. Phys. Acta **50**, 591 (1981).
[12] M. Nitta, J. Electrochem. Mater. **9**, 127 (1980).
[13] G. L. Smay and J. S. Wasylyk, Glass Tech. **22**, 2516 (1981).
[14] T. Ishida *et al.*, J. Electrochem. Soc. **141**, 1357 (1994).
[15] I. Bedja *et al.*, J. Appl. Phys. **75**, 5444 (1994).
[16] W. Fliegel *et al.*, Sens. Actuators B **19**, 474 (1994).
[17] T. S. Rantala *et al.*, Sens. Actuators B **19**, 716 (1994).
[18] K. N. Yu *et al.*, Nanostruct. Mater. **5**, 819 (1995).
[19] Y. H. Xiong, K. N. Yu, and C. S. Xiong, Phys. Rev. B **49**, 5607 (1994); **50**, 11 287 (1994).
[20] Powder Diffraction File, card 5-0467; Z. M. Jarzebski, *Oxide Semiconductors* (Pergamon, New York, 1973); p. 252; E. E. Kohnke, J. Phys. Solids **23**, 1557 (1962).
[21] T. Mutschele *et al.*, Scr. Metall. **21**, 135 (1987).
[22] J. F. Scott, J. Chem. Phys. **53**, 852 (1970).
[23] R. S. Katiyar *et al.*, J. Phys. C **4**, 2421 (1971); Phys. Lett. **25A**, 525 (1967).
[24] T. Sato *et al.*, J. Phys. Soc. Jpn. **64**, 1193 (1995).
[25] F. Gervais and W. Kress, Phys. Rev. B **31**, 4809 (1985).
[26] F. Matossi, J. Chem. Phys. **19**, 1543 (1951).
[27] W. Cochran, Adv. Phys. **19**, 387 (1960).
[28] C. Y. Xie, L. D. Zhang, and C. M. Mo, Phys. Status Solidi B **141**, 59 (1994).